Highlights of Spanish Astrophysics XII, Proceedings of the XVI Scientific Meeting of the Spanish Astronomical Society held on July 15 - 19, 2024, in Granada, Spain. M. Manteiga, F. González Galindo, A. Labiano Ortega, M. Martínez González, N. Rea, M. Romero Gómez, A. Ulla Miguel, G. Yepes, C. Rodríguez López, A. Gómez García and C. Dafonte (eds.), 2025

Quasar microlensing in galaxy clusters as a complementary approach to intracluster light

Forés-Toribio, R.[1,2], **Muñoz, J. A.**[1,2], **Fian, C.** [1,2] **Jiménez-Vicente, J.**[3,4] **and Mediavilla, E.** [5,6]

[1] Departamento de Astronomía y Astrofísica, Universidad de Valencia, E-46100 Burjassot, Valencia, Spain
[2] Observatorio Astronómico, Universidad de Valencia, E-46980 Paterna, Valencia, Spain
[3] Departamento de Física Teórica y del Cosmos, Universidad de Granada, Campus de Fuentenueva, 18071 Granada, Spain
[4] Instituto Carlos I de Física Teórica y Computacional, Universidad de Granada, 18071 Granada, Spain
[5] Instituto de Astrofísica de Canarias, Vía Láctea S/N, La Laguna, E-38200, Tenerife, Spain
[6] Departamento de Astrofísica, Universidad de la Laguna, La Laguna, E-38200, Tenerife, Spain

Abstract

In the gravitational lens SDSS J1004+4112, a background quasar is lensed by a galaxy cluster, hence the light from the quasar images travels mainly through the intracluster medium. Observations in the continuum emission and the broad line region detected variability due to microlensing in the multiple images of the quasar. In this work, we use the 14.5-year monitoring campaign in r-band and the time delays derived from these light curves by [19], to study their microlensing signature. We compare the observed microlensing differences between image pairs with Bayesian models to determine the stellar mass fractions at the image positions in the galaxy cluster and the quasar accretion disk size. We find a quasar half-light radius of $6.4^{+0.7}_{-0.3}\sqrt{M/0.3M_\odot}$ light-days at 2407Å in the rest frame, compatible with previous estimates. The stellar mass fractions at the four positions of the quasar images are $\alpha_A = 0.080^{+0.104}_{-0.018}$, $\alpha_B = 0.056^{+0.066}_{-0.032}$, $\alpha_C = 0.021^{+0.039}_{-0.021}$ and $\alpha_D = 0.072^{+0.063}_{-0.036}$. These estimates are compatible within 1σ with the expected fraction determined through intracluster light studies except for the first value, which is around 3σ discrepant. This may indicate the presence of an undetected stellar component in this region. Thus, quasar microlensing provides an independent probe of the intracluster medium and the extension to other lensing galaxy clusters will allow us to determine whether the inferences are compatible with direct observations of the intracluster light.

1 Introduction

The first example of a quasar lensed by a galaxy cluster was SDSS J1004+4112 discovered by [12]. Since the deflector mass is larger than for the typical scenario of lensed quasars, the multiple images are formed far (∼15”) from the brightest cluster galaxy. With this particular configuration, the light from the quasar images travels mainly through the intracluster medium and the impact of microlensing was expected to be small. However, soon after its discovery, microlensing variability was reported in the blue wing of the broad emission lines of image A ([21], [9], [16], [18], [3], [20] and [5]), as well as in the continuum emission of the accretion disk ([7], [1] and [4]).

Quasars exhibit intrinsic flux variability that needs to be removed in order to obtain the fluctuations produced only by microlensing. We used the light curves of the four brightest quasar images spanning 14.5 years and their time delays reported by [19] to subtract pairs of light curves shifted by their time delays and obtained light curves of the microlensing magnification differences. From these microlensing differences we inferred the accretion disk size of the quasar and the stellar mass fraction in the galaxy cluster where the images are located.

2 Methods and results

We smoothed the light curves with a window of ten days to reduce the noise and subtracted one light curve to another after shifting them by their corresponding time delays to remove the intrinsic quasar variability. We also subtracted their magnitudes in mid-infrared from [22] to correct for the macro-magnification since the mid-infrared emitting region of quasars is expected to be large enough to not be affected by microlensing. We constructed microlensing difference histograms by Monte Carlo sampling the six independent microlensing differences (A−B, C−B, D−B, A−C, D−C, and A−D) to account for observational errors and are presented in the left panel of Figure 1.

The histograms from observational data were fitted with model histograms that were obtained from magnification maps computed adopting the convergence and shear from the mass model of [8] and with variable fraction of mass in stars, α. The maps were convolved with different source sizes, $R_{1/2}$, modeled as Gaussians. We generated randomly oriented straight tracks for each image pair on its corresponding magnification map. We only kept the pairs of tracks whose average differs by less than 0.1 mag from the mean micro-magnification of the observed histograms to select regions with the proper underlying magnification. We collected 500 pairs of tracks that fulfill this condition, obtained their microlensing difference histograms and averaged them to obtain a single model histogram for each combination of parameters.

The probability that a given set of parameters reproduce the observed microlensing differences, H, is:

$$P(H|R_{1/2}, \alpha_A, \alpha_B, \alpha_C, \alpha_D) \propto e^{-\chi^2/2} \tag{1}$$

where

$$\chi^2 = \sum_{\mu} \sum_{i} \left(\frac{h_\mu(i) - \tilde{h}_\mu(i; R_{1/2}, \alpha_X, \alpha_R)}{\epsilon_\mu(i)} \right)^2 . \tag{2}$$

The first summation runs over the six microlensing differences and the second over the histogram bins. $h_\mu(i)$ is the ith bin of the normalised observed histogram, $\epsilon_\mu(i)$ is the error associated to that bin and $\tilde{h}_\mu(i; R_{1/2}, \alpha_X, \alpha_R)$ is ith bin of the difference of two model histograms for the given set of parameters.

The source size was sampled using logarithmically spaced values and the stellar mass fractions at images A, B, C, and D were varied in a range from 0 to 0.2. This range sets a flat prior on the stellar mass fractions to not exceed the average stellar mass fraction found for individual galaxies (see, e.g., [13]). The posterior distributions and the joint probabilities for each pair of parameters are presented in the right corner plot of Figure 1 and the reduced χ^2 is 0.997 for the best fit model histograms which are represented in the left panel of Figure 1 with solid black lines. We obtained an accretion disk size of $R_{1/2} = 6.4^{+0.7}_{-0.3}\sqrt{M/0.3M_\odot}$ light-days at 2407Å in the rest frame and the stellar mass fractions at the quasar image positions are $\alpha_A = 0.080^{+0.104}_{-0.018}$, $\alpha_B = 0.056^{+0.066}_{-0.032}$, $\alpha_C = 0.021^{+0.039}_{-0.021}$ and $\alpha_D = 0.072^{+0.063}_{-0.036}$.

3 Discussion and conclusions

When comparing our inferred value with previous size determinations at the same rest-frame wavelength and mean stellar mass, we found that our estimate is in tension with the determinations of [11], [17] and [7] who derived a smaller disk size. On the other hand, our value is compatible with the determinations of [6], [4], [14] and [18]. Given the length of the light curves, we achieve a tighter constraint on the source size than the majority of previous works.

Table 1: Estimates based on previous works for the stellar mass fraction from the brightest cluster galaxy and the intracluster light at the quasar image positions.

BCG+ICL	K18[15]	D18[2]	H20[10]
α_A	0.012 ± 0.007	0.006 ± 0.002	$0.012^{+0.022}_{-0.008}$
α_B	0.013 ± 0.008	0.007 ± 0.003	$0.013^{+0.025}_{-0.009}$
α_C	0.014 ± 0.009	0.008 ± 0.003	$0.011^{+0.022}_{-0.007}$
α_D	0.018 ± 0.010	0.038 ± 0.013	$0.022^{+0.028}_{-0.012}$

Regarding the stellar fraction estimates, we can compare them with the stellar contributions from the brightest cluster galaxy (BCG) and the intracluster light (ICL) at the specific quasar positions derived from [15], [2] and [10] (see Table 1). According to these estimations, α_B, α_C and α_D are compatible within 1σ with our inference but at the image position A we obtain a larger stellar mass fraction which is in a 3σ tension with ICL measurements. This may suggest the presence of an undetected additional stellar component in that region.

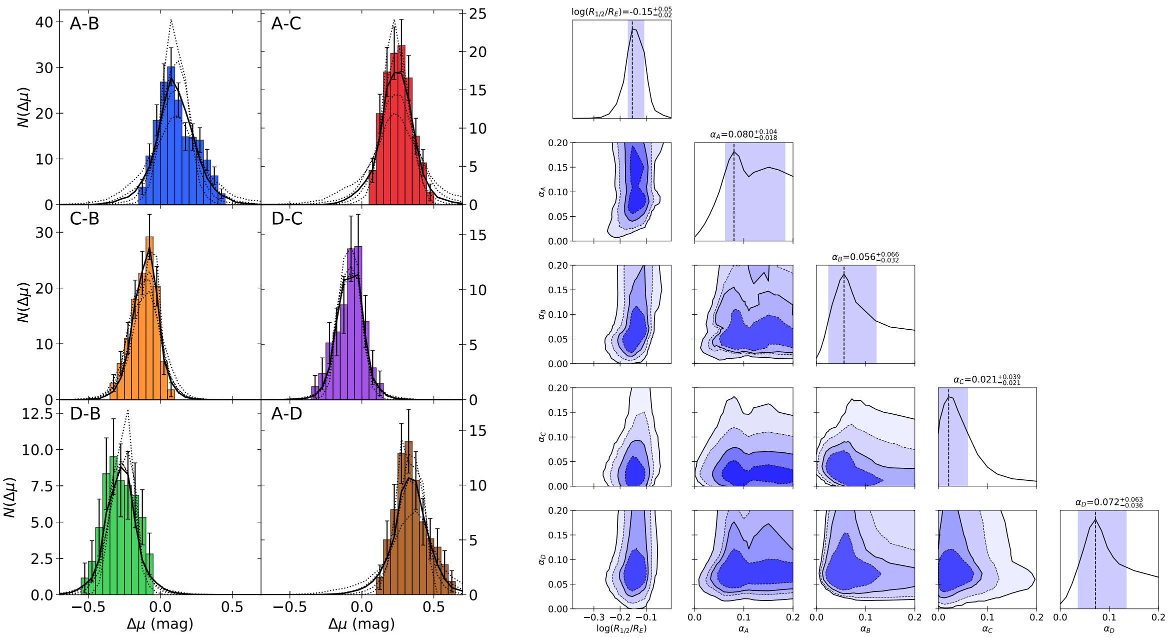

Figure 1: *Left panel:* Observed histograms of the six possible microlensing differences obtained after averaging the 10^6 realizations from the Monte Carlo sampling and the error bars are the standard deviation of these realizations. The solid black lines on top of the histograms represent the best model difference histograms and the thin dotted lines are model histograms whose χ^2 correspond to the 20th, 40th, 60th and 80th percentiles of the probability matrix. *Right panel:* Joint probability distributions by pairs of parameters and marginalized distributions for the five parameters ($R_{1/2}$, α_A, α_B, α_C and α_D). The confidence intervals are reported at the 68% confidence level around the maximum. In the 2D plots, the 1-σ and 2-σ contours are marked with solid lines and the 0.5-σ and 1.5-σ are displayed as dashed lines.

There are two other quasars lensed by galaxy clusters with measured time delays between some of their images, namely SDSS J1029+2623 and SDSS J2222+2745. Studying these two clusters will increase the statistics of stellar mass fractions at different cluster positions and properties of the intracluster medium can be inferred to evaluate the compatibility of microlensing determinations with those obtained through intracluster light observations. Additionally, the other four known cluster lens systems, and future discoveries of this particular lensing scenario, will provide an even larger sample of intracluster stellar mass fractions when the time delays between quasar images are determined.

Acknowledgments

This research was supported by the grants PID2020-118687GB-C31, PID2020-118687GB-C32 and PID2020-118687GB-C33 financed by the Spanish Ministerio de Ciencia e Innovación through MCIN/AEI/10.13039/501100011033. J.J.V. is also supported by projects FQM-108, P20_00334, and A-FQM-510-UGR20/FEDER, financed by Junta de Andalucía.

References

[1] Chen, B., Dai, X., Kochanek, C. S., et al. 2012, ApJ, 755, 24

[2] DeMaio, T., Gonzalez, A. H., Zabludoff, A., et al. 2018, MNRAS, 474, 3009

[3] Fian, C., Guerras, E., Mediavilla, E., et al. 2018, ApJ, 859, 50

[4] Fian, C., Mediavilla, E., Hanslmeier, A., et al. 2016, ApJ, 830, 149

[5] Fian, C., Mediavilla, E., Motta, V., et al. 2021, A&A, 653, A109

[6] Fian, C., Muñoz, J. A., Forés-Toribio, R., et al. 2024, A&A, 682, A57

[7] Fohlmeister, J., Kochanek, C. S., Falco, E. E., et al. 2008, ApJ, 676, 761

[8] Forés-Toribio, R., Muñoz, J. A., Kochanek, C. S., et al. 2022, ApJ, 937, 35

[9] Gómez-Álvarez, P., Mediavilla, E., Muñoz, J. A., et al. 2006, ApJL, 645, L5

[10] Henden, N. A., Puchwein, E., & Sijacki, D. 2020, MNRAS, 498, 2114

[11] Hutsemékers, D., Sluse, D., Savić, D., et al. 2023, A&A, 672, A45

[12] Inada, N., Oguri, M., Pindor, B., et al. 2003, Nature, 426, 810

[13] Jiménez-Vicente, J., Mediavilla, E., Kochanek, C. S.,& Muñoz, J. A. 2015, ApJ, 799, 149

[14] Jiménez-Vicente, J., Mediavilla, E., Kochanek, C. S., et al. 2014, ApJ, 783, 47

[15] Kravtsov, A. V., Vikhlinin, A. A., & Meshcheryakov, A. V. 2018, Astronomy Letters, 44, 8

[16] Lamer, G., Schwope, A., Wisotzki, L., et al. 2006, A&A, 454, 493

[17] Mosquera, A. M. & Kochanek, C. S. 2011, ApJ, 738, 96

[18] Motta, V., Mediavilla, E., Falco, E., et al. 2012, ApJ, 755, 82

[19] Muñoz, J. A., Kochanek, C. S., Fohlmeister, J., et al. 2022, ApJ, 937, 34

[20] Popović, L. Č., Afanasiev, V. L., Moiseev, A., et al. 2020, A&A, 634, A27

[21] Richards, G. T., Keeton, C. R., Pindor, B., et al. 2004, ApJ, 610, 679

[22] Ross, N. R., Assef, R. J., Kochanek, C. S., et al. 2009, ApJ, 702, 472